

**Muon sites in PbF<sub>2</sub> and YF<sub>3</sub>: Decohering environments and the role of anion Frenkel defects**J. M. Wilkinson <sup>1,\*</sup>, F. L. Pratt <sup>2</sup>, T. Lancaster <sup>3</sup>, P. J. Baker <sup>2</sup> and S. J. Blundell <sup>1,†</sup><sup>1</sup>*Clarendon Laboratory, University of Oxford Department of Physics, Parks Road, Oxford, OX4 3PJ, United Kingdom*<sup>2</sup>*ISIS Facility, STFC Rutherford Appleton Laboratory, Didcot OX11 0QX, United Kingdom*<sup>3</sup>*Department of Physics, Centre for Materials Physics, Durham University, Durham DH1 3LE, United Kingdom*

(Received 1 September 2021; revised 29 October 2021; accepted 7 December 2021; published 22 December 2021)

Muons implanted into ionic fluorides often lead to a so-called F- $\mu$ -F state, in which the time evolution of the muon spin contains information about the geometry and nature of the muon site. Nuclei more distant from the muon than the two nearest-neighbor fluorine ions result in decoherence of the F- $\mu$ -F system, and this can yield additional quantitative information about the state of the muon. We demonstrate how this idea can be applied to the determination of muon sites within the ionic fluorides  $\alpha$ -PbF<sub>2</sub> and YF<sub>3</sub>, which contain fluoride ions in different crystallographic environments. Our results can be used to distinguish between different crystal phases and provide strong evidence for the existence of anion Frenkel defects in  $\alpha$ -PbF<sub>2</sub>.

DOI: [10.1103/PhysRevB.104.L220409](https://doi.org/10.1103/PhysRevB.104.L220409)

Muon spin rotation ( $\mu$ SR) is a technique which involves implanting spin-polarized positive muons (lifetime  $\tau_\mu = 2.2 \mu\text{s}$ ) in samples to probe the local magnetic environment [1,2]. This technique has been applied very successfully to measure vortices in superconductors [3], explore the ground state of magnetic materials [4,5], probe the physics of hydrogen-like defect states in semiconductors [6–8] and in many other situations. To quantitatively analyze the data obtained from  $\mu$ SR experiments, one needs to know the final stopping site of the implanted muon within the crystal, and the extent to which the muon perturbs the local crystallographic and electronic structure. Density-functional theory (DFT) calculations have recently been used to address this question [9–11]. The muon is placed at a randomly chosen site in the unit cell and the structure relaxed, with all atoms and the muon allowed to move until convergence is reached and the final energy evaluated; repeating this for many initial muon positions and identifying the minimum-energy configuration yields an estimate of the muon site and allows the local distortions of the structure to be identified. This method is often referred to as “DFT +  $\mu$ .”

Ionic fluorides are a useful class of materials for the study of muon stopping sites and the muon-induced perturbation on the local crystallographic environment [9,12]. Fluorine, being the most electronegative element [13], is a very attractive atom for the incoming  $\mu^+$  and, in ionic fluorides, the muon commonly stops between two fluorine anions, adopting a F- $\mu$ -F state, somewhat analogous to a bifluoride ion (HF<sub>2</sub><sup>-</sup>). Following implantation, the muon spin becomes entangled with the spins on nearest-neighbor fluorine nuclei, and the muon’s polarization then evolves with time as governed by the magnetic dipolar Hamiltonian, producing a characteristic beating oscillatory signal in the measured positron asymmetry

[12,14] that allows the muon site to be identified. The muon’s polarization also decoheres into the environment (the spin system consisting of all the other nuclei in the compound), becoming lost in an irreversible process, which causes a relaxation in the beating oscillatory signal. It has been shown very recently that this can be quantitatively modeled to produce excellent agreement with experimental data in the simple cubic fluorides CaF<sub>2</sub> and NaF [15].

In this Letter, we extend the method used for CaF<sub>2</sub> and NaF [15] and apply it to two ionic fluorides: YF<sub>3</sub> [16] and  $\alpha$ -PbF<sub>2</sub>. These were chosen because they have structural phases with a more complicated structure than the simple cubic phases considered previously and thereby show that this method can be utilized in conjunction with DFT +  $\mu$  to provide an insight into structural phase transitions and defect states, allowing us to gain a fuller understanding of the nature of the perturbation of the muon on the surrounding nuclei.

When a muon is implanted in a sample, it interacts with the surrounding nuclear spins by means of the dipole-dipole Hamiltonian  $\mathcal{H}$ , given by

$$\mathcal{H} = \sum_{i>j} \frac{\mu_0 \gamma_i \gamma_j}{4\pi \hbar |\mathbf{r}_{ij}|^3} [\mathbf{s}_i \cdot \mathbf{s}_j - 3(\mathbf{s}_i \cdot \hat{\mathbf{r}}_{ij})(\mathbf{s}_j \cdot \hat{\mathbf{r}}_{ij})], \quad (1)$$

where  $\mathbf{r}_{ij}$  is the vector linking spins  $i$  and  $j$ , and all other symbols having their usual meanings [17]. For the case of a muon interacting with a spin- $\frac{1}{2}$  fluorine (<sup>19</sup>F) nucleus ( $\gamma_F = 2\pi \times 40.061 \text{ MHz T}^{-1}$ ), the muon’s polarization evolves in an observable pattern of beats (the frequencies of which provide information on the surrounding nuclei, due to the  $\mathbf{r}_{ij}$  dependence of the Hamiltonian), with a relaxation which is due to the system decohering with the environment of further nearest-neighbors, which have a weaker, but non-negligible coupling to the muon. Including all the nuclei in the sample directly in Eq. (1) is not possible since the dimension of  $\mathcal{H}$  grows exponentially with the number of spins included. Therefore, following Ref. [15] we cut off our Hilbert space

\*john.wilkinson@physics.ox.ac.uk

†stephen.blundell@physics.ox.ac.uk

to include enough nearest-neighbors to describe the main features of the  $\mu$ SR asymmetry and then rescale the coupling to the  $k$  ions most distant to the muon using a parameter  $\zeta_k$  which is chosen so that the second moment of our reduced system matches that of the infinite system. The variance of the field distribution at the muon site caused by  $M$  spins is  $(\sigma_M/\gamma_\mu)^2 = \frac{2}{3}(\frac{\mu_0}{4\pi})^2 \hbar^2 \sum_{j=1}^M \gamma_j^2 I_j(I_j + 1)/r_j^6$ , where  $r_j$  is the distance from the muon to the  $j$ th nucleus with spin  $I_j$  and gyromagnetic ratio  $\gamma_j$ ,  $\gamma_\mu (=2\pi \times 135.5 \text{ MHz T}^{-1})$  is the muon gyromagnetic ratio, and the sum converges as  $M \rightarrow \infty$ . We then calculate  $\zeta_k$  from

$$\sigma_\infty^2 = \sigma_{\text{nn}}^2 + \frac{2}{3} \left( \frac{\mu_0}{4\pi} \right)^2 \hbar^2 \gamma_\mu^2 \sum_{j \in k} \frac{\gamma_j^2 I_j(I_j + 1)}{(\zeta_k r_j)^6}, \quad (2)$$

and then evaluate our exact calculation of the muon polarization to the restricted set of muon, nearest-neighbors and the set of  $k$  ions (with the distance between the ion and the muon rescaled by  $\zeta_k$ ).

In many fluorides, an additional relaxation component is also present in the  $\mu$ SR asymmetry. The origin of this component has up until now been unidentified, but we believe that in  $\text{PbF}_2$  this is due to diamagnetic  $\text{Mu}^-$  states located in anion vacancies, the origin of which are due to anion Frenkel defects (AFDs). There have been a number of examples in the past of muons becoming trapped in vacancies in metallic systems, where the signature of the trapped muon is a change in the relaxation rate of the muon asymmetry. Fe [18] and quenched Al are classic examples of this effect, where for the latter case, the extra relaxation remains down to temperatures as low as 10 K [19]. These cases however relate to  $\mu^+$ , and requires significant muon diffusion in order for it to reach the vacancies [20]. On the other hand, in ionic fluorides, although  $\mu^+$  diffusion tends to require fairly high temperatures of about 200 K [21] due to the strength of the F- $\mu$ -F bonds, this is not necessarily the case for  $\text{Mu}^-$ .

The likelihood of AFDs forming is quantified by the defect formation energy  $g_F$ , which is usually of the order of a few eV, meaning that a large abundance of these defects often occur in equilibrium at temperatures of the order of hundreds of kelvin, but some can be ‘‘frozen in’’ to the material and therefore still be present at low temperatures. We utilized DFT to estimate the anion Frenkel defect formation energy, with an approach similar to that undertaken before in pyrochlores [22]: We created a supercell composed of  $2 \times 2 \times 2$  conventional unit cells, and one of the anions was displaced to a new site of high symmetry, and the cell relaxed. The location of the defects which had the lowest energy is shown in Fig. 1. We found that, if the anion is placed in an interstitial site sufficiently far away from the vacancy, the atoms would not relax to their original positions. The final relaxed energies of the supercells containing the defect were compared with those without defects to obtain an estimate for  $g_F$ , and these energies are tabulated in Table I alongside the experimental values where available, which agree well with our calculations. From this, one can conclude that both structural phases of  $\text{PbF}_2$  are much more likely to contain Frenkel defects than  $\text{YF}_3$  and  $\text{CaF}_2$ , a result which is supported by the absence of evidence of such defect states in those compounds in our  $\mu$ SR experiments.

We obtained samples of both  $\text{YF}_3$  and  $\text{PbF}_2$  commercially, and used an x-ray diffractometer to confirm that they did not contain any significant impurities (see Supplemental Material [23]) and that the  $\text{PbF}_2$  sample adopted the  $\alpha$  phase. These samples were then wrapped in silver foil and measured with the MuSR spectrometer at the ISIS facility [27]. The muon decay asymmetry was calculated from the number of counts in the forward and backward detectors, and high-statistics data were collected for both  $\text{YF}_3$  and  $\text{PbF}_2$  (274 and 358 million decay events, respectively).

The stopping sites of the muon were calculated using DFT +  $\mu$  for  $\text{YF}_3$ , and both the  $\alpha$  and  $\beta$  phases of  $\text{PbF}_2$  (see Supplemental Material for details [23]). The sites which had the lowest overall energy are depicted in Fig. 1 [28]. The stopping sites of the  $\text{Mu}^-$  ions in the vacancies caused by the AFDs were also calculated and are shown in the figure; they were found to be very close to the positions of the anion vacancies, as expected. The  $\text{PbF}_2$  data were fit with the function

$$A(t) = A_r[(1 - c_{\text{AFD}})P^\mu(r_{\text{nn1}}, r_{\text{nn2}}, r_{\text{nnn1}}, r_{\text{nnn2}}, \zeta_4; t) + c_{\text{AFD}}P^{\text{Mu}^-}(t)] + A_{\text{bg}}e^{-(\lambda t)^2}, \quad (3)$$

assuming the  $\alpha$  phase and also, to test the robustness of the procedure, assuming the  $\beta$  phase. The first term  $P^\mu(\dots)$  describes the muon polarization calculated from the dipolar Hamiltonian (1), using the muon site calculated with DFT +  $\mu$ , where  $r_{\text{nn1}}$  and  $r_{\text{nn2}}$  represent the distance from the muon to the two nearest-neighbor fluorines, and  $r_{\text{nnn1}}$  and  $r_{\text{nnn2}}$  are the distances to the next-nearest-neighbor fluorines. The second term  $P^{\text{Mu}^-}(t)$  is the polarization of the negatively charged muonium ion in an AFD site, and the final term  $e^{-(\lambda t)^2}$  represents a slow relaxation of the muon polarization due to the weak nuclear moments in the Ag sample holder. Because Pb has a very weak moment (the only isotope with spin,  $^{207}\text{Pb}$ , has  $\mu = 0.584\mu_N$  with 23% abundance), only the nearest ten fluorine nuclei were included in the calculation of the muon polarization (see the Supplemental Material for the positions of the included nuclei [23]) and so the Hamiltonian was described by a matrix of size  $2048 \times 2048$ .

The results of the fits to both the  $\alpha$  and  $\beta$  phases are shown in Fig. 2(a), along with simulations for which  $c_{\text{AFD}}$  was fixed to zero (i.e., ignoring AFDs). From this, one can see that the best fit is obtained including the presence of AFDs and with  $\text{PbF}_2$  adopting the  $\alpha$  phase. The superiority of the  $\alpha$ -phase fit is especially apparent for the data at longer times ( $>8 \mu\text{s}$ ), where the polarization function strongly deviates from the data for the  $\beta$  phase. Further evidence supporting the validity of the model applying to the  $\alpha$  phase of the compound is obtained by considering the second moment rescaling factor  $\zeta$ . The fit for the  $\alpha$  phase obtained a value of  $\zeta_4 = 0.834(5)$ , very close to the calculated value of 0.838. However, for the  $\beta$  phase, the fitted value of  $\zeta_{\text{nnn}} = 0.804(4)$  strongly deviates from the calculated value of 0.896. The structural distortions obtained from this fit, and the comparison to the values obtained with DFT +  $\mu$ , are in Table II. To test our hypothesis of  $\text{Mu}^-$  stopping in AFDs, we also used DFT +  $\mu$  to calculate the effect of another possible  $\text{Mu}^-$  state, which is in the pristine (defect-free)  $\text{PbF}_2$  lattice. In this case, the  $\text{Mu}^-$  finds a 4c site, with position  $(0.25, \frac{3}{4}, 0.274)$ , but the resulting

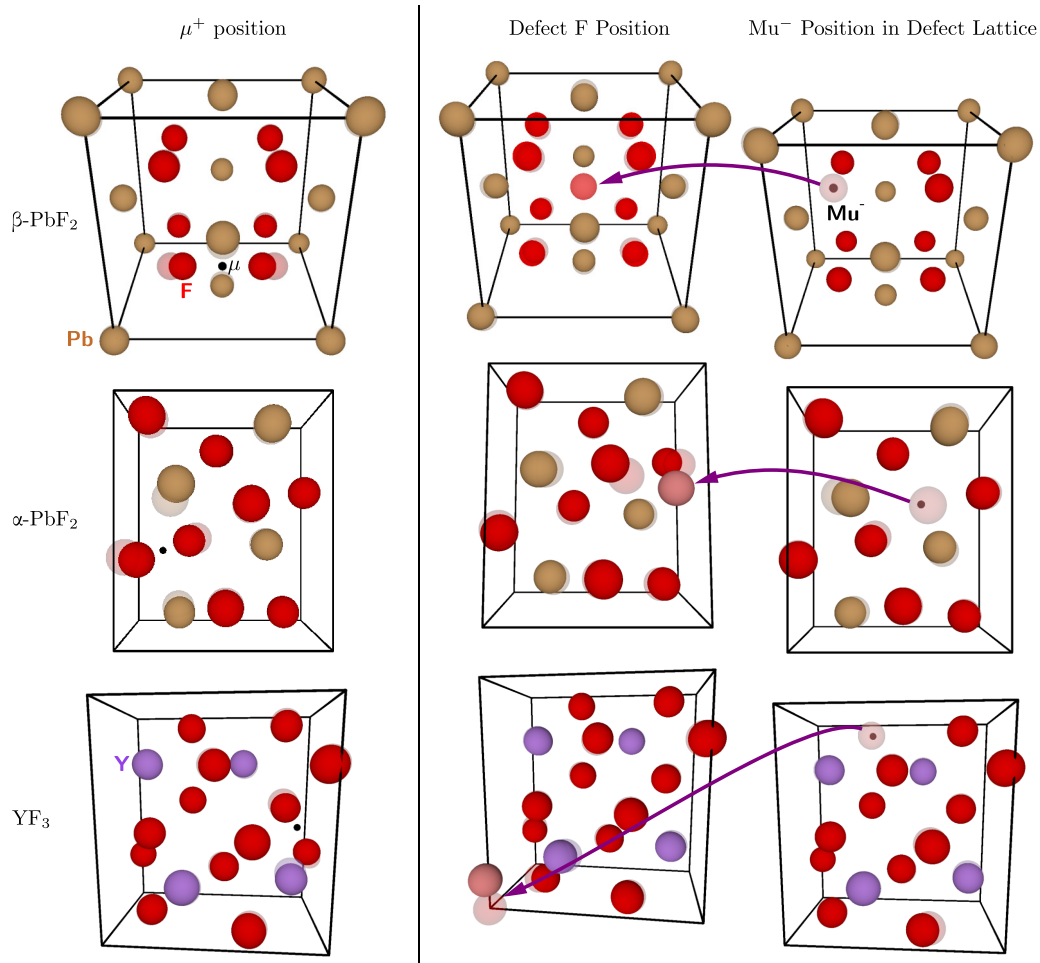


FIG. 1. Muon sites in PbF<sub>2</sub> and YF<sub>3</sub>, calculated with DFT. The left-hand side shows the muon site calculated with the DFT +  $\mu$  method, as described in the text. In all cases, the muon (black sphere) sits in between two fluoride ions (red spheres), and the transparent (solid) spheres show the locations of the surrounding ions before (after) the perturbation of the implanted muon. The center column shows the position of the defect fluorine in the perfect lattice, and the final (initial) relaxed positions of the surrounding ions are displayed as solid (transparent) spheres. Finally, the right-hand column shows the site of the  $\text{Mu}^-$  (black sphere) in the vacancy created by such a defect, and the effect of this on the surrounding ions.

muon polarization (plotted in the Supplemental Material [23]) relaxes rather quickly due to the stronger coupling between the muon and the fluoride ions, in disagreement with our data. The slower relaxation found for the  $\text{Mu}^-$  state in the AFD matches well with the slow background relaxation observed in the data (the nearest F to the  $\text{Mu}^-$  in the AFD state is 2.78 Å away, but for  $\text{Mu}^-$  in the perfect lattice the nearest fluorine is 2.29 Å away, a difference which nearly doubles

the leading-order term of the Hamiltonian), providing strong evidence for the presence of AFDs in our sample. Our results demonstrate that the details of the oscillatory signal are able to correctly distinguish between the two related crystallographic phases of PbF<sub>2</sub> and also determine the origin of the diamagnetic muonium signal. Note that the sensitivity of  $\mu\text{SR}$  data to these local differences is only revealed clearly in the late-time data (obtained well after  $\approx 5\tau_\mu$  where, because of the muon

TABLE I. Anion Frenkel defect energies  $g_F$  calculated by DFT (also showing the experimental values where available, using the method described in the text).

Compound	$g_F$ (eV) (calculated)	$g_F$ (eV) (experimental)
YF <sub>3</sub>	3.70	
CaF <sub>2</sub>	2.17	2.2–3.1 [24,25]
$\alpha\text{-PbF}_2$	1.55	1.12 [26]
$\beta\text{-PbF}_2$	1.05	0.9–1.1 [24,26]

TABLE II. Muon-induced structural distortions in PbF<sub>2</sub>, comparing the values obtained with the fit to experimental data with the values obtained using DFT +  $\mu$ .

Parameter	Experimental	DFT + $\mu$	Difference
$r_{\text{nn1}}$ (Å)	1.1419(4)	1.0967	+0.0452
$r_{\text{nn2}}$ (Å)	1.2601(7)	1.2057	+0.0544
$r_{\text{nnn1}}$ (Å)	2.68(3)	2.89	-0.21
$r_{\text{nnn2}}$ (Å)	3.01(7)	3.27	-0.26
$\zeta_4$	0.834(5)	0.838	-0.004

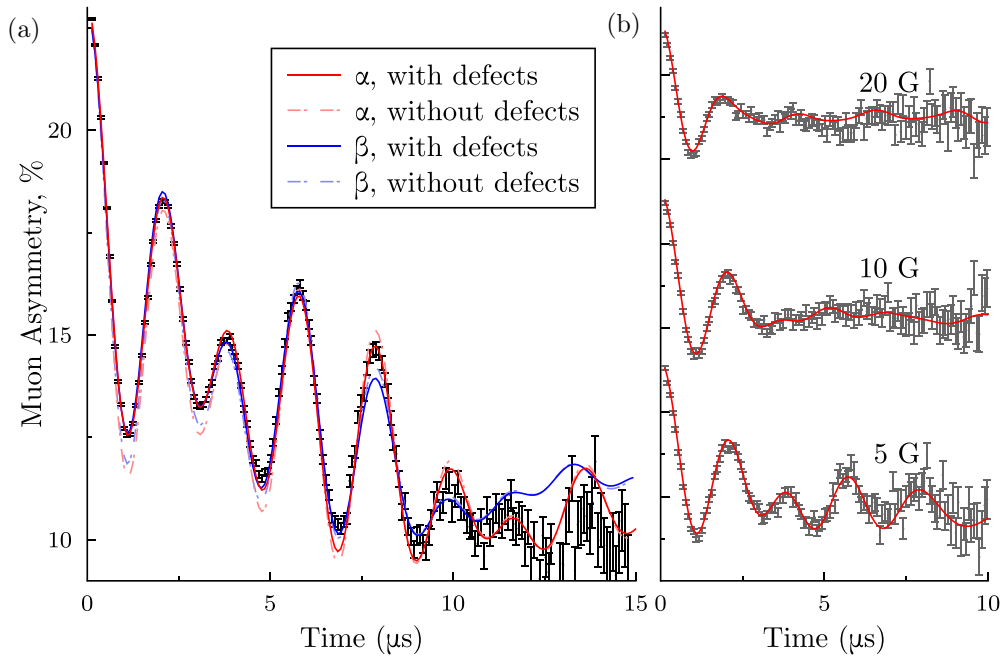


FIG. 2.  $\alpha$ -PbF<sub>2</sub> Results. (a) shows the zero-field  $\mu$ SR data obtained for our sample of PbF<sub>2</sub>, and the solid (dashed) lines corresponding to fits of the data with (without) taking into account the  $\text{Mu}^-$  entering into a defect state. (b) shows the data obtained with a longitudinal field applied, plotted with the muon polarization as described in the text.

decay, the data rate is more than two orders of magnitude lower than that obtained immediately after implantation). This result highlights the necessity for obtaining high-statistics  $\mu$ SR data so that these small late-time features in the data can be carefully resolved.

The best fit to the zero-field data was obtained assuming that 9.2(2)% of the diamagnetic fraction of the signal in  $\alpha$ -PbF<sub>2</sub> was due to AFD states. To further quantify the effect of these weak diamagnetic states, we applied a series of small longitudinal fields to the sample. Applying such fields adds an additional Zeeman term to the Hamiltonian, which, for AFD  $\text{Mu}^-$  states, tends to be much larger than the dipole interactions, and hence  $P^{\text{Mu}^-}(t) \approx 1$ . These results, along with plots of the polarization function for  $\alpha$ -PbF<sub>2</sub>, using parameters obtained from the aforementioned fit and including the longitudinal field, are shown in Fig. 2(b). One can see that our model continues to describe the data very well, and the field indeed removes much of the effect of the defect states on the polarization (which would not happen to the same extent for  $\text{Mu}^-$  in a pristine crystal because the dipole interactions are stronger). Distinguishing between  $\text{Mu}^-$  and  $\mu^+$  states, however, is notoriously difficult because there is no intrinsic spectroscopic difference between the two [29]. Previous studies [30,31] have found  $\text{Mu}^-$  states forming at temperatures of around 200 K and above; however, there is some experimental evidence of a  $\text{Mu}^-$  state forming in H-doped perovskites at temperatures as low as 15 K [32]. This state was discovered by observing the  $\text{Mu}^-$ -H dipole entanglement, extracting the muon-H bond length and finding it to be too large to be due to a  $\mu$ -H state [32], a somewhat analogous situation to the case of  $\alpha$ -PbF<sub>2</sub> considered here.

As our data for YF<sub>3</sub> did not show any slow relaxing background, and the DFT results show that AFDs are less likely to form than in PbF<sub>2</sub>, we did not need to include AFDs in our

fits of the data. Therefore, we fit our YF<sub>3</sub> data to a simpler functional form given by

$$A(t) = A_r P^\mu(r_{\text{nn}1}, r_{\text{nn}2}, r_{\text{nnn}1}, r_{\text{nnn}2}, \zeta_6; t) + A_{\text{bg}}, \quad (4)$$

where all symbols have the same meaning as before. As with PbF<sub>2</sub>, the ten nearest fluorine nuclei were included in the calculation (Y has only one natural isotope, <sup>89</sup>Y, with a negligible moment of 0.137  $\mu_N$ ), leading again to matrices of size 2048  $\times$  2048 (see the Supplemental Material for the details of the included nuclei [23]). The site which was predicted by DFT to have the lowest energy (using both the LDA and PBE functionals) was used to calculate the muon polarization, the fit of which is depicted as the green line in Fig. 3. The values obtained from the fit, and their DFT counterparts, are tabulated in Table III, where it can be seen that the nearest- and next-nearest-neighbor perturbations of the fluorines due to the muon are in excellent agreement.

Note that, for both the measured muon-induced distortions of PbF<sub>2</sub> and YF<sub>3</sub>, the discrepancy between the DFT values and the fitted values increases with the muon-fluorine distance, and that DFT slightly underestimates the bond lengths for

TABLE III. Muon-induced structural distortions in YF<sub>3</sub>, comparing the values obtained with the fit to experimental data with the values obtained using DFT +  $\mu$ .

Parameter	Experimental	DFT + $\mu$	Difference
$r_{\text{nn}1}$ (Å)	1.173(1)	1.10	+0.073
$r_{\text{nn}2}$ (Å)	1.278(2)	1.22	+0.058
$r_{\text{nnn}1}$ (Å)	2.24(3)	2.15	+0.09
$r_{\text{nnn}2}$ (Å)	2.40(1)	2.49	-0.09
$\zeta_6$	0.849(5)	0.907	-0.058

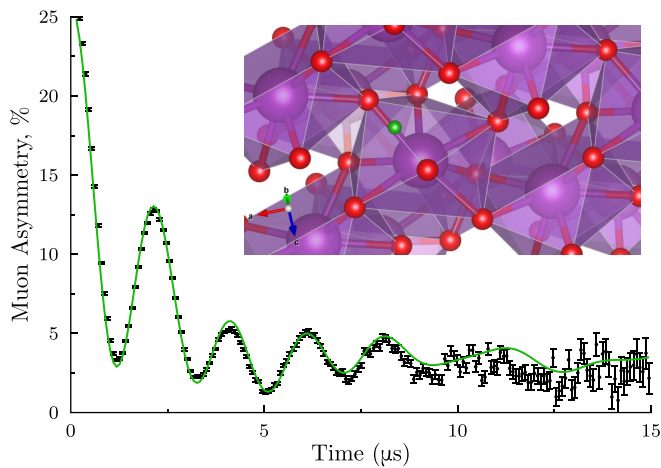


FIG. 3. YF<sub>3</sub> results: The results of our  $\mu$ SR experiment, with the fitted muon polarization using the muon site obtained by DFT. This site is displayed on the YF<sub>3</sub> crystal structure in the inset, with the atom positions unperturbed for simplicity.

nuclei close to the muon and slightly overestimates these for those nuclei further away. While the PBE functionals tend to slightly underestimate bond lengths, the effect further from the muon may be due to the size of the supercell.

In conclusion, we have shown how the analysis of  $\mu$ SR data on complex fluorides allows one to obtain a wealth of useful information about the muon stopping site and the environment of the muon, information which was previously not obtainable when phenomenological relaxation functions were used to analyze the data. We have also shown how the longer-time data are particularly useful for understanding the nature of the muon site. Additionally, we have shown that it is possible to measure anion Frenkel defects using  $\mu$ SR in a model system, an important result which can be extended to the analysis of magnetic systems, where the effects of defects on the electronic structure could be important.

We acknowledge support from EPSRC (Grant No. EP/N023803/1) and the use of the University of Oxford Advanced Research Computing (ARC) facility in carrying out this work [38]. We are grateful to D. Prabhakaran for performing the x-ray measurement and to Marina Filip and Pietro Bonfà for useful discussions. Experiments at the ISIS Neutron and Muon Source were supported by a beamtime allocation RB1920547 from the Science and Technology Facilities Council.

- [1] S. J. Blundell, Spin-polarized muons in condensed matter physics, *Contemp. Phys.* **40**, 175 (1999).
- [2] *Introduction to Muon Spectroscopy*, edited by S. J. Blundell, R. De Renzi, T. Lancaster, and F. L. Pratt (Oxford University Press, Oxford, 2022).
- [3] J. E. Sonier, J. H. Brewer, and R. F. Kiefl,  $\mu$ SR studies of the vortex state in type-II superconductors, *Rev. Mod. Phys.* **72**, 769 (2000).
- [4] P. D. de R otier and A. Yaouanc, Muon spin rotation and relaxation in magnetic materials, *J. Phys.: Condens. Matter* **9**, 9113 (1997).
- [5] F. L. Pratt, P. J. Baker, S. J. Blundell, T. Lancaster, S. Ohira-Kawamura, C. Baines, Y. Shimizu, K. Kanoda, I. Watanabe, and G. Saito, Magnetic and non-magnetic phases of a quantum spin liquid, *Nature (London)* **471**, 612 (2011).
- [6] B. D. Patterson, Muonium states in semiconductors, *Rev. Mod. Phys.* **60**, 69 (1988).
- [7] S. F. J. Cox, Muonium as a model for interstitial hydrogen in the semiconducting and semimetallic elements, *Rep. Prog. Phys.* **72**, 116501 (2009).
- [8] K. Shimomura and T. U. Ito, Electronic structure of hydrogen donors in semiconductors and insulators probed by muon spin rotation, *J. Phys. Soc. Jpn.* **85**, 091013 (2016).
- [9] J. S. M oller, D. Ceresoli, T. Lancaster, N. Marzari, and S. J. Blundell, Quantum states of muons in fluorides, *Phys. Rev. B* **87**, 121108(R) (2013).
- [10] F. Bernardini, P. Bonf a, S. Massidda, and R. De Renzi, *Ab initio* strategy for muon site assignment in wide band gap fluorides, *Phys. Rev. B* **87**, 115148 (2013).
- [11] P. Bonf a and R. De Renzi, Toward the computational prediction of muon sites and interaction parameters, *J. Phys. Soc. Jpn.* **85**, 091014 (2016).
- [12] T. Lancaster, S. J. Blundell, P. J. Baker, M. L. Brooks, W. Hayes, F. L. Pratt, J. L. Manson, M. M. Conner, and J. A. Schlueter, Muon-Fluorine Entangled States in Molecular Magnets, *Phys. Rev. Lett.* **99**, 267601 (2007).
- [13] A. L. Allred, Electronegativity values from thermochemical data, *J. Inorg. Nucl. Chem.* **17**, 215 (1961).
- [14] J. H. Brewer, S. R. Kreitzman, D. R. Noakes, E. J. Ansaldo, D. R. Harshman, and R. Keitel, Observation of muon-fluorine “hydrogen bonding” in ionic crystals, *Phys. Rev. B* **33**, 7813 (1986).
- [15] J. M. Wilkinson and S. J. Blundell, Information and Decoherence in a Muon-Fluorine Coupled System, *Phys. Rev. Lett.* **125**, 087201 (2020).
- [16] Although YF<sub>3</sub> has been measured and analyzed before [10], the crystal structure used for the analysis was incorrect, and it was therefore not possible in that study to fit the data without including a phenomenological relaxation function.
- [17] For nuclei which have a spin greater than  $\frac{1}{2}$ , an additional quadrupolar term would also need to be included in the Hamiltonian.
- [18] A. M oslang, H. Graf, G. Balzer, E. Recknagel, A. Weidinger, T. Wichert, and R. I. Grynspan, Muon trapping at monovacancies in iron, *Phys. Rev. B* **27**, 2674 (1983).
- [19] J. A. Brown, R. H. Heffner, M. Leon, M. E. Schillaci, D. W. Cooke, and W. B. Gauster, Trapping of Positive Muons at Vacancies in Quenched Aluminium, *Phys. Rev. Lett.* **43**, 1513 (1979).
- [20] K. Dorenburg, M. Gladisch, D. Herlach, W. Mansel, H. Metz, H. Orth, G. zu Putlitz, A. Seeger, W. Wahl, and M. Wingand, Trapping by vacancies and mobility of positive muons in neutron-irradiated aluminium, *Z. Phys. B: Condens. Matter* **31**, 165 (1978).

- [21] J. H. Brewer, D. R. Harshman, R. Keitel, S. R. Kreitzman, G. M. Luke, D. R. Noakes, and R. E. Turner, Thermal hopping of  $\mu^+$  between “F $\mu$ F” centres in NaF, *Hyperfine Interact.* **32**, 677 (1986).
- [22] W. R. Panero, L. P. Stixrude, and R. C. Ewing, First-principles calculation of defect-formation energies in the Y<sub>2</sub>(Ti, Sn, Zr)<sub>2</sub>O<sub>7</sub> pyrochlore, *Phys. Rev. B* **70**, 054110 (2004).
- [23] See Supplemental Material at <http://link.aps.org/supplemental/10.1103/PhysRevB.104.L220409> for details of the experiment, information regarding the muon polarization simulations and investigations of other potential muon sites.
- [24] V. P. Zhukov and V. M. Za, First-principles calculations of the electronic structure of fluorite-type crystals and transport properties, *Phys. Solid State* **40**, 1827 (1998).
- [25] W. Mackrodt, Defect Calculations for Ionic Materials, in *Computer Simulation of Solids* (Springer-Verlag, Berlin, 1982), Chap. 12, p. 175.
- [26] G. A. Samara, Pressure and temperature dependences of the ionic conductivities of cubic and orthorhombic lead fluoride (PbF<sub>2</sub>), *J. Phys. Chem. Solids* **40**, 509 (1979).
- [27] Data for this study are available from doi: [10.5286/ISIS.E.RB1920547](https://doi.org/10.5286/ISIS.E.RB1920547).
- [28] There were some additional sites for  $\alpha$ -PbF<sub>2</sub> and YF<sub>3</sub> which had energy only a few meV above these, but the muon polarization due to these sites are not realized in the data. See Supplemental Material [23] for details, which contains the additional references [33–37].
- [29] T. U. Ito, W. Higemoto, and K. Shimomura, Negatively charged muonium and related centres in solids, *J. Phys. Soc. Jpn.* **89**, 051007 (2020).
- [30] K. H. Chow, R. F. Kiefl, W. A. MacFarlane, J. W. Schneider, D. W. Cooke, M. Leon, M. Paciotti, T. L. Estle, B. Hitti, R. L. Lichti, S. F. J. Cox, C. Schwab, E. A. Davis, A. Morrobel-Sosa, and L. Zavieh, Structure of negatively charged muonium in *n*-type GaAs, *Phys. Rev. B* **51**, 14762 (1995).
- [31] K. Shimomura, R. Kadono, A. Koda, K. Nishiyama, W. Hugemoto, and T. U. Ito,  $\mu$ Sr Study on Isolated Hydrogen and Oxygen Vacancy in SrTiO<sub>3</sub>, *JPS Conf. Proc.* **2**, 010308 (2014).
- [32] T. U. Ito, A. Koda, K. Shimomura, W. Higemoto, T. Matsuzaki, Y. Kobayashi, and H. Kageyama, Excited configurations of hydrogen in the BaTiO<sub>3-x</sub>H<sub>x</sub> perovskite lattice associated with hydrogen exchange and transport, *Phys. Rev. B* **95**, 020301(R) (2017).
- [33] D. R. Noakes, E. J. Ansaldo, S. R. Kreitzman, and G. M. Luke, the (F $\mu$ F)<sup>-</sup> ion in solid fluorides, *J. Phys. Chem. Solids* **54**, 785 (1993).
- [34] Y. Ito and K. Koto, Thermal hysteresis of anion disorder in beta-PbF<sub>2</sub>, *Solid State Ionics* **9-10**, 527 (1983).
- [35] A. Zalkin and D. H. Templeton, The crystal structures of YF<sub>3</sub> and related compounds, *J. Am. Chem. Soc.* **64**, 2453 (1953).
- [36] L. Ehm, K. Knorr, F. Madler, H. Voigtlander, E. Busetto, A. Cassetta, A. Lausi, and B. Winkler, High-pressure X-ray diffraction study on  $\alpha$ -(PbF<sub>2</sub>), *J. Phys. Chem. Solids* **64**, 919 (2003).
- [37] P. Giannozzi, S. Baroni, N. Bonini, M. Calandra, R. Car, C. Cavazzoni, D. Ceresoli, G. L. Chiarotti, M. Cococcioni, I. Dabo, A. D. Corso, S. de Gironcoli, S. Fabris, G. Fratesi, R. Gebauer, U. Gerstmann, C. Gougoussis, A. Kokalj, M. Lazzeri, L. Martin-Samos *et al.*, QUANTUM ESPRESSO: A modular and open-source software project for quantum simulations of materials, *J. Phys.: Condens. Matter* **21**, 395502 (2009).
- [38] <http://dx.doi.org/10.5281/zenodo.22558>.